

## Experimental setup of the $^{239}\text{Pu}$ neutron capture and fission cross-section measurements at n\_TOF, CERN

Adrian Sanchez-Caballero<sup>2,\*</sup>, Victor Alcayne<sup>2</sup>, Józef Andrzejewski<sup>6</sup>, Daniel Cano-Ott<sup>2</sup>, Thomas Cardinaels<sup>49</sup>, Peter Dries<sup>49</sup>, Aleksandra Gawlik-Ramięga<sup>6</sup>, Enrique González-Romero<sup>2</sup>, Jan Heyse<sup>34</sup>, Gregory Leinders<sup>49</sup>, Trinitario Martínez<sup>2</sup>, Emilio Mendoza<sup>2</sup>, Andre Moens<sup>34</sup>, Alberto Pérez de Rada<sup>2</sup>, Jarosław Perkowski<sup>6</sup>, Arjan Plompen<sup>34</sup>, Carlos Paradela<sup>34</sup>, Peter Schillebeeckx<sup>34</sup>, Goedele Sibbens<sup>34</sup>, Karen Van Hecke<sup>49</sup>, Koen Vanaken<sup>49</sup>, David Vanleeuw<sup>34</sup>, Ken Verguts<sup>49</sup>, Marc Verwerft<sup>49</sup>, Ruud Wynants<sup>34</sup>, Oliver Aberle<sup>1</sup>, Saverio Altieri<sup>3,4</sup>, Simone Amaducci<sup>5</sup>, Victor Babiano-Suarez<sup>7</sup>, Michael Bacak<sup>1</sup>, Javier Balibrea Correa<sup>7</sup>, Chiara Beltrami<sup>3</sup>, Samuel Bennett<sup>8</sup>, Ana-Paula Bernardes<sup>1</sup>, Eric Berthoumieux<sup>9</sup>, Roland Beyer<sup>10</sup>, Marian Boromiza<sup>11</sup>, Damir Bosnar<sup>12</sup>, Manuel Caamaño<sup>13</sup>, Francisco Calviño<sup>14</sup>, Marco Calviani<sup>1</sup>, Adria Casanovas<sup>14</sup>, Donato Castelluccio<sup>15,16</sup>, Francesco Cerutti<sup>1</sup>, Gabriele Cescutti<sup>17,18</sup>, Sotirios Chasapoglou<sup>19</sup>, Enrico Chiaveri<sup>1,8</sup>, Paolo Colombari<sup>20,21</sup>, Nicola Colonna<sup>22</sup>, Patrizio Console Camprini<sup>16,15</sup>, Guillem Cortés<sup>14</sup>, Miguel Cortés-Giraldo<sup>23</sup>, Luigi Cosentino<sup>5</sup>, Sergio Cristallo<sup>24,25</sup>, Dellmann<sup>26</sup>, Mario Di Castro<sup>1</sup>, Salvatore Di Maria<sup>27</sup>, Maria Diakaki<sup>19</sup>, Mirco Dietz<sup>28</sup>, César Domingo-Pardo<sup>7</sup>, Rüdiger Dressler<sup>29</sup>, Emmeric Dupont<sup>9</sup>, Ignacio Durán<sup>13</sup>, Zinovia Eleme<sup>30</sup>, Sylvain Fargier<sup>1</sup>, Begoña Fernández<sup>23</sup>, Beatriz Fernández-Domínguez<sup>13</sup>, Paolo Finocchiaro<sup>5</sup>, Salvatore Fiore<sup>15,31</sup>, Walter Furman<sup>32</sup>, Francisco García-Infantes<sup>33,1</sup>, Gianpiero Gervino<sup>20,21</sup>, Simone Gilardon<sup>1</sup>, Carlos Guerrero<sup>23</sup>, Frank Gunsing<sup>9</sup>, Carlo Gustavino<sup>31</sup>, William Hillman<sup>8</sup>, David Jenkins<sup>35</sup>, Erwin Jericha<sup>36</sup>, Arnd Junghans<sup>10</sup>, Yacine Kadi<sup>1</sup>, Kalliopi Kaperoni<sup>19</sup>, Gurpreet Kaur<sup>9</sup>, Atsushi Kimura<sup>37</sup>, Ingrid Knapová<sup>38</sup>, Michael Kokkoris<sup>19</sup>, Yury Kopatch<sup>32</sup>, Milan Krtička<sup>38</sup>, Nikolaos Kyritsis<sup>19</sup>, Ion Lăărescu<sup>7</sup>, Claudia Lederer-Woods<sup>39</sup>, Jorge Lerendegui-Marco<sup>7</sup>, Giuseppe Lerner<sup>1</sup>, Alice Manna<sup>16,40</sup>, Alessandro Masi<sup>1</sup>, Cristian Massimi<sup>16,40</sup>, Pierfrancesco Mastinu<sup>41</sup>, Mario Mastromarco<sup>22,42</sup>, Emilio-Andrea Maugeri<sup>29</sup>, Annamaria Mazzone<sup>22,43</sup>, Alberto Mengoni<sup>15,16</sup>, Veatriki Michalopoulou<sup>19</sup>, Paolo Milazzo<sup>17</sup>, Riccardo Mucciola<sup>24,44</sup>, Fabrizio Murtas<sup>†45</sup>, Elizabeth Musacchio-Gonzalez<sup>41</sup>, Agatino Musumarra<sup>46,47</sup>, Alexandru Negret<sup>11</sup>, Pablo Pérez-Maroto<sup>23</sup>, Nikolas Patronis<sup>30,1</sup>, José-Antonio Pavón-Rodríguez<sup>23,1</sup>, Maria Pellegriti<sup>46</sup>, Cristina Petrone<sup>11</sup>, Elisa Pirovano<sup>28</sup>, Julio Plaza del Olmo<sup>2</sup>, Stephan Pomp<sup>48</sup>, Ignacio Porras<sup>33</sup>, Javier Praena<sup>33</sup>, José-Manuel Quesada<sup>23</sup>, René Reifarth<sup>26</sup>, Dimitri Rochman<sup>29</sup>, Yuriy Romanets<sup>27</sup>, Carlo Rubbia<sup>1</sup>, Marta Sabaté-Gilarte<sup>1</sup>, Dorothea Schumann<sup>29</sup>, Adhitya Sekhar<sup>8</sup>, Gavin Smith<sup>8</sup>, Nikolay Sosnin<sup>39</sup>, Maria-Elisso Stamati<sup>30,1</sup>, Alessandro Sturniolo<sup>20</sup>, Giuseppe Tagliente<sup>22</sup>, Ariel Tarifeño-Saldivia<sup>14</sup>, Diego Tarriño<sup>48</sup>, Pablo Torres-Sánchez<sup>33</sup>, Vagena<sup>30</sup>, Stanislav Valenta<sup>38</sup>, Vincenzo Variale<sup>22</sup>, Pedro Vaz<sup>27</sup>, Gianfranco Vecchio<sup>5</sup>, Diego Vescovi<sup>26</sup>, Vasilis Vlachoudis<sup>1</sup>, Rosa Vlastou<sup>19</sup>, Anton Wallner<sup>10</sup>, Philip-John Woods<sup>39</sup>, Tobias Wright<sup>8</sup>, Roberto Zarrella<sup>16,40</sup>, and Petar Žugec<sup>12</sup>

and the n\_TOF Collaboration

<sup>1</sup>European Organization for Nuclear Research (CERN), Switzerland

<sup>2</sup>Centro de Investigaciones Energéticas Medioambientales y Tecnológicas (CIEMAT), Spain

<sup>3</sup>Istituto Nazionale di Fisica Nucleare, Sezione di Pavia, Italy

\*e-mail: adrian.sanchez@ciemat.es

<sup>4</sup>Department of Physics, University of Pavia, Italy<sup>5</sup>INFN Laboratori Nazionali del Sud, Catania, Italy<sup>6</sup>University of Lodz, Poland<sup>7</sup>Instituto de Física Corpuscular, CSIC - Universidad de Valencia, Spain<sup>8</sup>University of Manchester, United Kingdom<sup>9</sup>CEA Irfu, Université Paris-Saclay, F-91191 Gif-sur-Yvette, France<sup>10</sup>Helmholtz-Zentrum Dresden-Rossendorf, Germany<sup>11</sup>Horia Hulubei National Institute of Physics and Nuclear Engineering, Romania<sup>12</sup>Department of Physics, Faculty of Science, University of Zagreb, Zagreb, Croatia<sup>13</sup>University of Santiago de Compostela, Spain<sup>14</sup>Universitat Politècnica de Catalunya, Spain<sup>15</sup>Agenzia nazionale per le nuove tecnologie (ENEA), Italy<sup>16</sup>Istituto Nazionale di Fisica Nucleare, Sezione di Bologna, Italy<sup>17</sup>Istituto Nazionale di Fisica Nucleare, Sezione di Trieste, Italy<sup>18</sup>Department of Physics, University of Trieste, Italy<sup>19</sup>National Technical University of Athens, Greece<sup>20</sup>Istituto Nazionale di Fisica Nucleare, Sezione di Torino, Italy<sup>21</sup>Department of Physics, University of Torino, Italy<sup>22</sup>Istituto Nazionale di Fisica Nucleare, Sezione di Bari, Italy<sup>23</sup>Universidad de Sevilla, Spain<sup>24</sup>Istituto Nazionale di Fisica Nucleare, Sezione di Perugia, Italy<sup>25</sup>Istituto Nazionale di Astrofisica - Osservatorio Astronomico di Teramo, Italy<sup>26</sup>Goethe University Frankfurt, Germany<sup>27</sup>Instituto Superior Técnico, Lisbon, Portugal<sup>28</sup>Physikalisch-Technische Bundesanstalt (PTB), Bundesallee 100, 38116 Braunschweig, Germany<sup>29</sup>Paul Scherrer Institut (PSI), Villigen, Switzerland<sup>30</sup>University of Ioannina, Greece<sup>31</sup>Istituto Nazionale di Fisica Nucleare, Sezione di Roma1, Roma, Italy<sup>32</sup>Affiliated with an institute covered by a cooperation agreement with CERN<sup>33</sup>University of Granada, Spain<sup>34</sup>European Commission, Joint Research Centre (JRC), Geel, Belgium<sup>35</sup>University of York, United Kingdom<sup>36</sup>TU Wien, Atominstitut, Stadionallee 2, 1020 Wien, Austria<sup>37</sup>Japan Atomic Energy Agency (JAEA), Tokai-Mura, Japan<sup>38</sup>Charles University, Prague, Czech Republic<sup>39</sup>School of Physics and Astronomy, University of Edinburgh, United Kingdom<sup>40</sup>Dipartimento di Fisica e Astronomia, Università di Bologna, Italy<sup>41</sup>INFN Laboratori Nazionali di Legnaro, Italy<sup>42</sup>Dipartimento Interateneo di Fisica, Università degli Studi di Bari, Italy<sup>43</sup>Consiglio Nazionale delle Ricerche, Bari, Italy<sup>44</sup>Dipartimento di Fisica e Geologia, Università di Perugia, Italy<sup>45</sup>INFN Laboratori Nazionali di Frascati, Italy<sup>46</sup>Istituto Nazionale di Fisica Nucleare, Sezione di Catania, Italy<sup>47</sup>Department of Physics and Astronomy, University of Catania, Italy<sup>48</sup>Department of Physics and Astronomy, Uppsala University, Box 516, 75120 Uppsala, Sweden<sup>49</sup>SCK CEN, Belgian Nuclear Research Centre, Boeretang 200, Mol, B-2400, Belgium

**Abstract.** The experimental setup of the new measurement of  $^{239}\text{Pu}$  fission and capture cross-section in the n\_TOF time-of-flight facility at CERN is presented. The measurement aims to address the needs and demands of nuclear data users. The experiment incorporates an innovative fast Fission Fragment Detector and the n\_TOF Total Absorption Calorimeter, enabling the implementation of the fission tagging technique. Preliminary results exhibit the robust performance of the detector systems, along with the high quality of the new  $^{239}\text{Pu}$  samples.

These samples were exclusively produced for this measurement by the European Commission's Joint Research Centre in Geel.

## 1 Introduction

As the usage and development of nuclear technologies continue to expand, so does the demand for precise and reliable nuclear data. In particular, more accurate neutron-induced fission and capture cross-section data for  $^{239}\text{Pu}$  are required for the design of novel critical nuclear systems, such as Generation-IV reactors [1] and Accelerator Driven Systems (ADS), and for the operation of current thermal reactors loaded with *mixed oxide* (MOX) fuels. Due to the limited experimental data available and the discrepancies among the main evaluated nuclear databases [2–6], new measurements of the capture and fission cross-section of  $^{239}\text{Pu}$  are highly recommended, as it is included in the NEA/OECD High Priority Request List [7].

Only two measurements of the  $^{239}\text{Pu}$  capture cross-section have been reported with enough energy resolution to perform a reasonable resonance analysis in the resolved resonance region. The first one was performed by Gwin et al. [8] in 1971, covering the neutron energy range between 0.02 eV and 30 keV. The second one was performed in 2014 by Mosby et al. [9–11] at the Los Alamos Neutron Science Center using the DANCE detector, for neutron energies from 10 eV to 1.3 MeV. In the latter, only the shape of the cross-section was measured, i.e. it was normalized to the ENDF/B-VII.1 [6] cross section at 17–18 eV.

In this work, a new recent measurement of the  $^{239}\text{Pu}$  capture and fission cross-section performed at the neutron time-of-flight facility *n\_TOF* [12] at CERN is presented. The experiment was performed in the 185 m experimental area *EAR1*. This flight path is nearly 10 times larger than the ones used for previous  $^{239}\text{Pu}$  capture measurements, enabling a potential improvement in the energy resolution of the measured cross-sections. To accomplish this, the collaborating groups have made use of the expertise obtained in previous capture measurements of fissile samples [13–15] to design a new improved experimental setup, which consists in the simultaneous operation of the *n\_TOF* Total Absorption Calorimeter (TAC) [16], already used in previous measurements, and a new fast fission fragment detector (FFD) specifically fabricated for this experiment.

The rest of this publication is organized as follows. In Section 2, the main properties of the  $^{239}\text{Pu}$  samples used in this work are described. A detailed overview of the novel Fast Fission Detector is given in Section 3, and a general description of the two experimental setups, in Section 4. Finally, some preliminary results are shown in Section 5, along with the conclusions in Section 6.

## 2 The $^{239}\text{Pu}$ samples

Two different experimental configurations were used. First, ten thin samples and the FFD were used to efficiently subtract the fission background between 0.02 eV to 1 keV. Reaching higher neutron energies in this configuration, in the case of the capture cross-section, is limited by the low statistics and high background. For this reason, a *thicker* sample was utilized in the second experimental configuration without the FFD to reach higher neutron energies at least up to 10 keV (limited also by the gamma-flash effect in the  $\text{BaF}_2$  crystals of the TAC).

Therefore, a total of 11  $\text{PuO}_2$  samples were manufactured at the European Commission Joint Research Centre (JRC-Geel, Belgium) for this experiment. Ten samples, each of them with a mass lower than 1 mg, were deposited in aluminum foils with 10  $\mu\text{m}$  thickness (see left picture in Figure 1) and hold by aluminum rings that were placed inside the fission chamber.

**Table 1.** Properties of the  $^{239}\text{Pu}$  targets inside the fission chamber used in the n\_TOF experiment.

Target position	Activity (MBq)	Mass ( $\mu\text{g}$ )	Areal density ( $\mu\text{g}/\text{cm}^2$ )
1	2.24	975	310
2	2.22	965	307
3	2.20	959	305
4	2.09	911	290
5	0.28	122	39
6	1.94	844	268
7	2.19	953	303
8	2.11	920	293
9	2.09	912	290
10	2.25	982	312

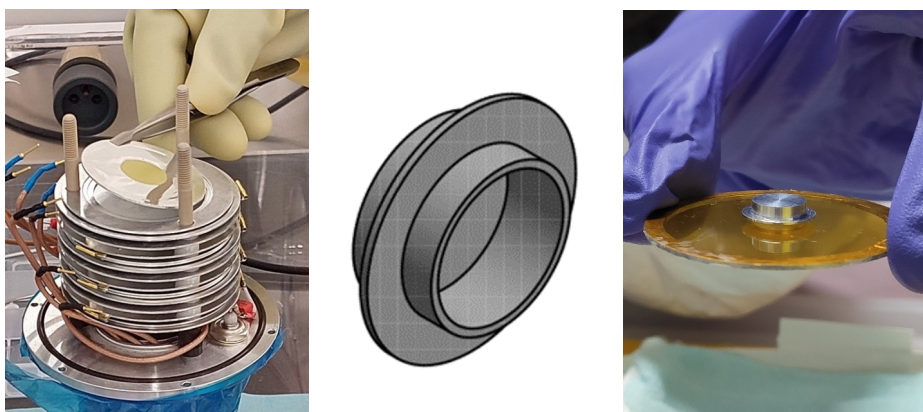


**Figure 1.** Left: picture of the mounting process of one  $\text{PuO}_2$  sample in the fission chamber. Middle: design of the aluminum capsule for the  $^{239}\text{Pu}$  thick target. Right: picture of the actual capsule containing the thick sample during its mounting between two aluminum rings with kapton and mylar foils (the top mylar ring does not appear in this picture).

Some physical properties of these samples are shown in Table 1. Additionally, a thicker target of 101.69 mg was produced and encapsulated in a two-piece *hat*-shaped aluminum structure (see Figure 1, central and right image). The *hat*-shaped structure minimizes the possible movements of the sample powder inside the capsule. The same adhesive used to join these two pieces was utilized for another identical aluminum capsule without plutonium, which was necessary for the background characterization in dedicated measurements.

### 3 The fission fragment detector

The new FFD is a multi-section ionization fission chamber. Its main purpose is to serve as a veto for fission events registered in the TAC. In addition, the FFD was used to measure the  $^{239}\text{Pu}(n,\text{f})$  cross-section.

The design of the FFD was optimized to ensure: i) a good discrimination between alpha particles coming from the radioactive decay of  $^{239}\text{Pu}(n,\text{f})$  and the fission fragments emitted in the nuclear fission reactions, ii) a high time resolution to minimize pile-up effects mainly due to the high counting rate from the alpha-decays (around  $10^6$  counts/s), and iii) as high a

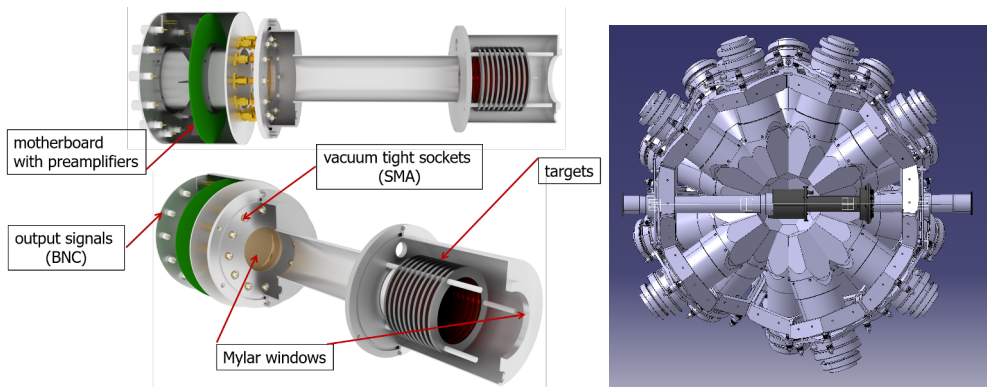


**Figure 2.** Left: a simplified 3D model of the fast fission fragment detector with the attachable aluminum box which houses the motherboard with the preamplifiers. Some critical elements inside the chamber, such as the aluminum electrodes or cables are omitted. Right: a 3D model of the fast fission fragment detector mounted inside the TAC. One half of the TAC is hidden for visualization purposes. The neutron beam would be coming from left in the image.



**Figure 3.** Photographs of the experimental setup of the  $^{239}\text{Pu}$  measurement at n\_TOF. Left: mounting of the Li-doped polyethylene neutron absorber surrounding the FFD, located at the center of the TAC. Middle: modified version of the dummy fission chamber with the thick plutonium sample for the second experimental configuration, before mounting inside the TAC. Right: top view of the  $^{239}\text{Pu}$  thick sample in the modified dummy fission chamber.

fission detection efficiency as possible, determined by the restrained dimensions to fit within the 10 cm inner radius of the TAC (see right image in Figure 2).

The ten  $^{239}\text{Pu}$  targets were placed on the cathodes of ten parallel plate ionization detectors arranged within a cylindrical chamber. This design eliminates potential cross-talk or interdependence between plates, enabling separately detection of the fission fragments from each target. A gas mixture of 90% Ar and 10%  $\text{CF}_4$  continuously flows through the chamber, selected to provide the shortest rise times of the registered signals.

An aluminum box containing some electronics is placed outside the central space but still inside the TAC assembly structure, and is attached to the FFD, as can be seen on the left hand side of the left image in Figure 2. This chamber contains the necessary preamplifiers to obtain

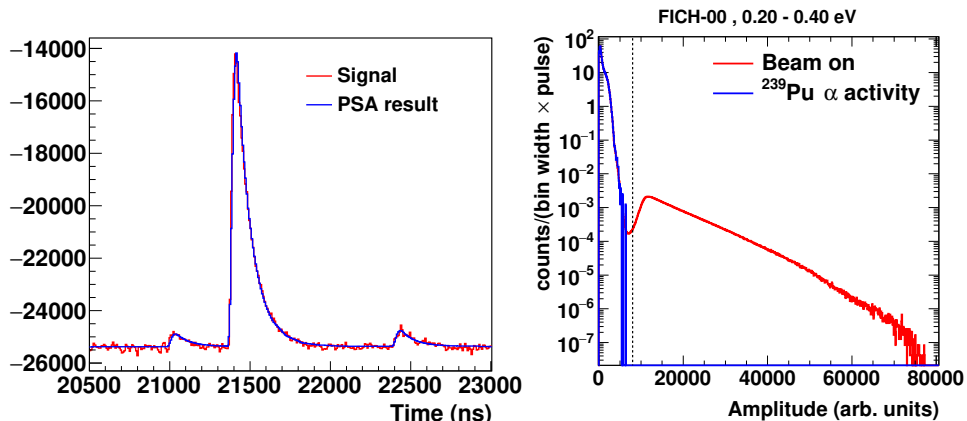


**Figure 4.** Left: a digitized signal from the FFD in red and the result of the fit of the PSA routine in blue. The y-axis is in arbitrary units. Right: amplitude spectra of measurements with (red) and without (blue) beam, representing the fission fragments and decay alphas, respectively, for events of neutron energies between 0.2 and 0.4 eV.

the desired properties for the electrical signals. Following these preamplifiers, the signals go through an analogue fast amplifier before reaching the n\_TOF digitalization system [17].

An identical *dummy* fission chamber was built without the plutonium targets to characterize the beam-related background of the measurement. This *dummy* chamber was also used, after some modifications, as the supporting structure of the thick sample for the second experimental configuration.

## 4 Description of the two experimental setups

As previously mentioned, two different experimental setups were used. In the first configuration, both the TAC and the FFD were utilized to simultaneously measure the capture and fission cross-section of ten  $^{239}\text{Pu}$  thin samples, housed within the main chamber of the FFD. To measure capture, the fission tagging technique [18] was employed by detecting fission events with the FFD, thereby determining the  $\gamma$ -ray fission background registered in the TAC crystals. Due to the neutron sensitivity of  $\text{BaF}_2$  crystals, a Li-doped polyethylene neutron absorber was built to minimize the neutron background originating from fission and scattering processes. The neutron absorber comprises two matching halves, with the interior tailored to the geometry of the FFD chamber (see left picture in Figure 3 which shows one half being installed).

In the second experimental configuration, the encapsulated thick  $^{239}\text{Pu}$  sample was employed for measuring the capture cross-section above 1 keV with the TAC. Positioning the sample within the beam trajectory while maintaining stability, alignment, and minimizing dead material effects, was done by using the dummy fission chamber. To mitigate background from the dead material of the dummy FFD, some elements such as cables, aluminum plates, structural pieces, etc. were removed, as they are not necessary for this configuration. This new version of the dummy fission chamber (without the aluminum cap for visualization purposes) is displayed in the middle image of Figure 3. The thick sample was placed in a fixed position corresponding to the estimated center of the TAC. A top view of the encapsulated sample in its definitive position within the chamber can be seen in the right image of Figure 3.

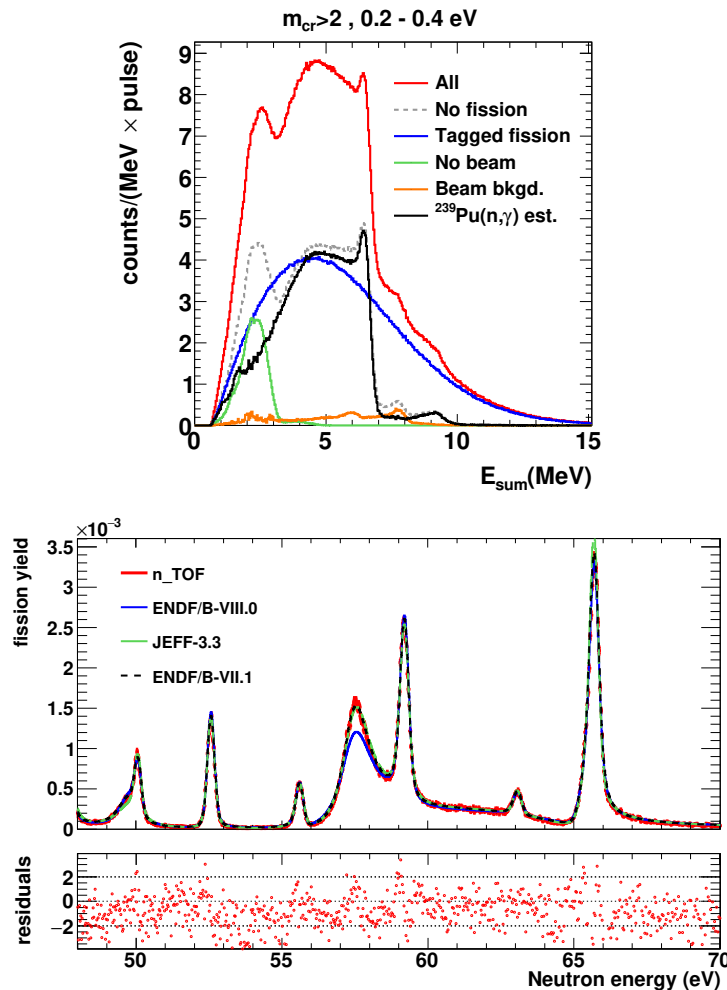


**Figure 5.** Top: total deposited energy spectra in the TAC showing the different contributions (see text for more details). Bottom: example of the preliminary fission yield obtained with the FFD compared with main nuclear data evaluations.

The assembly process was similar to the first configuration, including the same neutron absorber shown in the left image of Figure 3.

## 5 First results

An example of a characteristic digitized signal of the FFD is shown in the left panel of Figure 4. A big signal from a fission fragment is observed, accompanied by two small signals most likely originated by alpha particles from the decay of  $^{239}\text{Pu}$ . The result of the fit by the Pulse Shape Analysis (PSA) routine, shown in blue, is used to discriminate between alphas and fission fragments, as can be seen in the right panel of Figure 4. The vertical dashed line represents a possible threshold to select the fission fragments for the data analysis. The comparison of the amplitude spectrum with a measurement without beam shows that the overlap

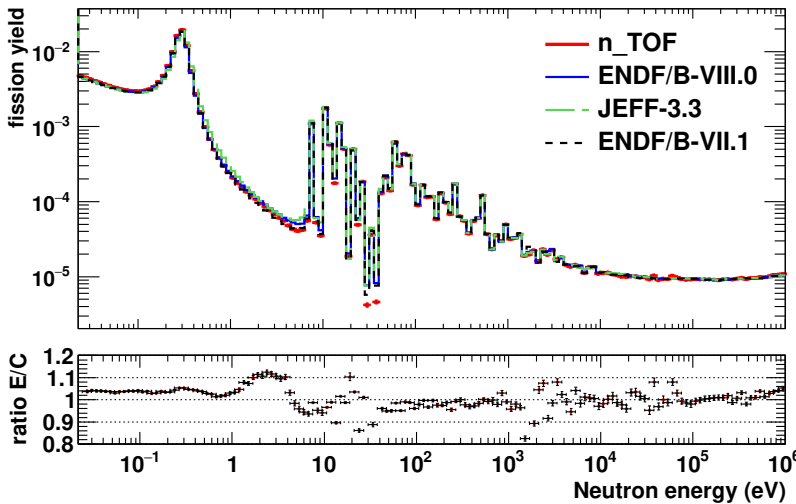


**Figure 6.** Preliminary integrated fission yield with 20 bins per decade. The ratio of n\_TOF data relative to ENDF/B-VII.1 is also shown below. The error bars represent only the statistical uncertainties.

between alpha particles and fission fragments is minimal, thus enabling a good discrimination between particles.

The measured fission events with the FFD are correlated in time with the events in the TAC, obtaining the prompt fission gamma background in the BaF<sub>2</sub> crystals. The tagged fission in the TAC is displayed in the top panel of Figure 5 as the blue curve together with different contributions to the events detected in the TAC. This plot includes only events with more than 2 BaF<sub>2</sub> crystals contributing to the total deposited energy in the TAC, commonly known as crystal multiplicity ( $m_{cr}$ ). This restriction in the TAC events has been used in previous measurements to minimize uncorrelated background as ambient activity (see green line in Figure 5) and other background sources that emit one or two gamma rays. The amplitude spectrum of all the events registered in the TAC under this condition is represented by the red line in Figure 5. The gray dashed line is obtained by subtracting the fission background. The beam related background, measured with the dummy version of the fission chamber with no sample, is displayed by the orange curve. When all these background contributions are subtracted, the solid black line is obtained as an estimation of the neutron capture spectrum in the TAC. Some events above 6.5 MeV -the neutron separation energy of <sup>240</sup>Pu- are still present, and will be studied and subtracted in the final version of the analysis. We attribute this contribution mainly to neutrons emitted in (n,f) reactions detected out of the TAC-FFD time coincidence window.

An example of a preliminary fission yield obtained with the FFD compared with the yields from three different evaluations with the n\_TOF resolution function is shown in the bottom panel of Figure 5. In general, a better agreement with the ENDF/B-VII.1 evaluation is observed. For this reason, the residuals are calculated relative to ENDF/B-VII.1.

The preliminary integrated fission yield with 20 bins per decade is shown in Figure 6. As a first approach, the n\_TOF data has been normalized to the evaluated ENDF/B-VII.1 yield in the neutron energy range 17-18 eV, as done in previous measurements [9-11]. A good agreement is observed along the complete range of neutron energy between 0.02 eV and

almost 1 MeV. Some corrections are still needed and are currently under investigation. For instance, the neutron flux in the region below 4 eV has to be determined with more precision.

## 6 Conclusion

A new measurement of the neutron fission and capture cross-section of  $^{239}\text{Pu}$  has been performed in the neutron time-of-flight facility n\_TOF at CERN to fulfill the nuclear data demand and requirements by the nuclear technologies. A detailed description of the experimental setups used for this measurement is given in this publication. Although the data analysis is still ongoing, some preliminary results have been presented.

## 7 Acknowledgements

This project has received funding from the Euratom research and training programme 2014-2018 under grant agreement No 847594 (ARIEL). This work was supported in part by the European Commission through the H2020 Framework Programme under grant agreement No 847552 and the 2021-1-RD EUFRAT-GELINA project, and by the I+D+i grants PGC2018-096717-B-C21, PID2021-123100NB-I00 and PDC2021-120828-I00 funded by MCIN/AEI/10.13039/501100011033. This research was also funded in part by National Science Centre, Poland (Grant No. UMO-2021/41/B/ST2/00326).

## References

- [1] M. Salvatores et al., *International Evaluation Co-operation. Volume 26* (OECD Publishing, Paris, 2008) 465.
- [2] N. Otuka et al., Nucl. Data Sheets **120**, 272-276 (2014)
- [3] D.A. Brown, Nucl. Data Sheets **148**, 1-142 (2018)
- [4] A. Plompen et al., Eur. Phys. J. A **56**, 1-108 (2020)
- [5] K. Shibata et al., J. Nucl. Sci. Technol. **48**, 1046-1051 (2011)
- [6] M. B. Chadwick et al., Nucl. Data Sheets **112**, 2887 (2011)
- [7] E. Dupont et al., EPJ Web Conf. **239**, 15005 (2020)
- [8] Gwin et al., Nucl. Sci. Eng. **45**, 25 (1971)
- [9] S. Mosby et al., Phys. Rev. C **89**, 034610 (2014)
- [10] S. Mosby et al., Phys. Rev. C **97**, 041601 (2018)
- [11] S. Mosby et al., Nucl. Data Sheets **148**, 312-321 (2018)
- [12] C. Guerrero et al., Eur. Phys. J. A **49**, 27 (2013)
- [13] J. Balibrea-Correa et al., Phys. Rev. C **102**, 044615 (2020)
- [14] M. Bacak, et al., EPJ Web Conf. **239**, 01043 (2020)
- [15] F. Belloni et al., Eur. Phys. J. A **47**, 2 (2011)
- [16] C. Guerrero et al., Nucl. Instrum. Methods A **608** 3, 424-433 (2009)
- [17] U. Abbondanno et al., Nucl. Instrum. Methods A **538** 1-3, 692-702 (2005)
- [18] G. de Saussure et al., *Nuclear Data for Reactors: Proceedings of a Conference on Nuclear Data, Microscopic Cross Sections, and Other Data Basic for Reactors* (IAEA, Vienna, 1967), 437